# OPTICS VERSUS COMPUTATION: INFLUENCE OF ILLUMINATION AND RECONSTRUCTION MODEL ACCURACY IN FOCAL-PLANE-SCANNING OPTICAL PROJECTION TOMOGRAPHY

*François Marelli*[1,2], *Michael Liebling*[1,3]

[1]Idiap Research Institute, CH-1920 Martigny, Switzerland
[2]École Polytechnique Fédérale de Lausanne (EPFL), CH-1015 Lausanne, Switzerland
[3]Electrical & Computer Engineering, University of California, Santa Barbara, CA 93106, USA

## ABSTRACT

Optical Projection Tomography (OPT) imaging provides isotropic resolution for samples up to a few millimeters. High resolution OPT is achieved by deconvolving Focal-Plane-Scanning (FPS-OPT) data but it requires to accurately know the system's Point Spread Function (PSF). While the presence of noise and inaccuracies in the PSF model or parameters affects reconstruction quality, their effect is difficult to assess quantitatively in practice and the computational cost of naive simulations is prohibitively expensive. Here, we present an efficient approach to carry out FPS-OPT simulations for a wide range of illumination geometries, including Focal-Sheet-Scanning OPT (FSS-OPT), a method using a lateral light-sheet illumination to perform FPS-OPT. We implement a simulation framework that can accomodate large size 3D data by dividing the forward model into elements that can be efficiently processed by GPUs. We compare the performance of FPS-OPT and FSS-OPT on simulated data. In the presence of Poisson noise, we show that FSS-OPT outperforms FPS-OPT with deconvolution even if all model parameters are accurately known. We then validate these results on experimentally acquired data. The availability of an efficient 3D OPT simulation framework for quantitative comparison of imaging scenarios is an essential tool for determining efficient imaging geometries to evaluate the relative benefits of computational and hardware variations.

***Index Terms***— Optical Projection Tomography, Light Sheet Fluorescence Microscopy, Optical Microscopy

## 1. INTRODUCTION

Optical Projection Tomography (OPT) is a microscopy technique used for 3D imaging of mesoscopic samples, from a few micrometers to a few millimeters [1]. It uses projected images taken at different angles to reconstruct volumetric information, similarly to X-ray computed tomography. To achieve approximately straight-line projections, OPT requires the sample to be smaller than the imaging depth of field. Low Numerical Aperture (NA) objectives have a large depth of field and are typically used for OPT but they have worse lateral resolution thereby limiting the resolution of OPT systems.

In order to circumvent this limitation, the depth of field of high-NA objectives can be extended by scanning the focal plane through the sample, creating high-resolution pseudoprojections [2]. A 3D image is then reconstructed from these projections using the Filtered BackProjection (FBP) [3]. The pseudoprojections contain blurred out-of-focus information, which can be filtered out to further improve the quality of the reconstruction [4, 5]. This filtering operation requires to know the Point Spread Function (PSF) of the system, but measuring it is very difficult in practice [6].

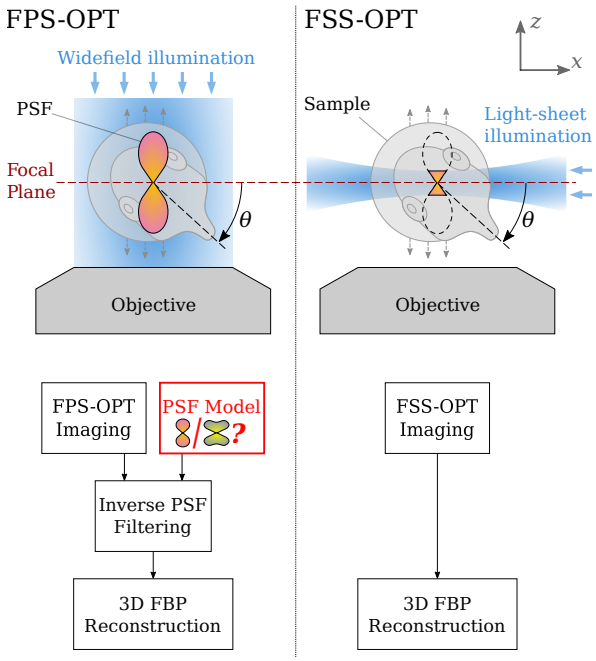


**Fig. 1**. Comparison of FPS-OPT and FSS-OPT focal plane scanning OPT methods. In both methods, the sample is rotated then scanned along the $z$ axis to get pseudoprojections. FPS-OPT allows taking into account high-NA PSFs in a traditional wide-field illumination acquisition setup; precise reconstruction requires a modified filtered back-projection and knowledge of the PSF. FSS-OPT uses an optically more involved lateral light-sheet illumination setup that truncates the PSF sufficiently for direct reconstruction with X-ray tomography-like methods.

In this paper, we propose to combine Light-Sheet Fluorescence Microscopy (LSFM) [7] with focal plane scanning in order to reduce out-of-focus blur for high-NA objectives, into Focal-Sheet-Scanning OPT (FSS-OPT). Specifically, we present a simulation framework to compare its performance to the Focal-Plane-Scanning OPT (FPS-OPT) technique described in [5], which implements a modified FBP incorporating deconvolution to take into account the PSF. Our aim is to measure the impact that potential errors on the precise PSF have during FPS-OPT's reconstruction and whether it remains competitive with the (all-optical) FSS-OPT technique.

In Section 2, we present the imaging processes and the reconstruction algorithms. In Section 3, we characterize the methods us-

ing a 3D phantom with different NAs, and describe the implementation of an efficient framework used for the simulations. In Section 4, we illustrate the results on OPT data from fluorescent textile fibre.

## 2. IMAGING METHODS

Focal-plane scanning OPT methods, such as the method proposed by Miao et al. [2], use data obtained via pseudoprojections, that is, by integrating the images obtained when scanning the focal plane through the whole sample. In practice, this is done by taking a single long exposure image while sweeping the focal plane through the object, or by acquiring a depth stack of the sample and averaging the images. This scanning procedure is common to both FPS-OPT and FSS-OPT, which we will describe shortly.

For the following, let $f(x, y, z)$ be a 3D object to be imaged, with $x, y, z$ the horizontal, vertical and focus axes, respectively; and $y$ is used as the rotation axis for the acquisitions.

### 2.1. FPS-OPT

We briefly recall FPS-OPT [2, 5], which uses wide-field imaging to acquire the projections, as illustrated in Figure 1. The entire sample is illuminated, and $p(s, y, \theta)$, the pseudoprojection acquired at an angle $\theta$, results from a convolution between the object and the hourglass-shaped PSF of the system $h(x, y, z)$ according to:

$$p(s, y, \theta) = \mathcal{X}f \circledast \left\{ \int_{\mathbb{R}} h(x, y, z)\, \mathrm{d}z \right\} = \mathcal{X}f \circledast h_{\perp}(x, y), \quad (1)$$

where $\circledast$ is a convolution on the first two axes, and $h_{\perp}(x, y)$ is the projection of the PSF along $z$; $\mathcal{X}f(s, y, \theta)$ is the 2D projection of $f$ along the direction $\theta$ using to the X-ray transform, with $s$ the horizontal axis in projected space, and $\delta(\cdot)$ the Dirac delta function:

$$\mathcal{X}f(s, y, \theta) = \iint_{\mathbb{R}^2} f(x, y, z)\, \delta(z\cos(\theta) + x\sin(\theta) - s)\, \mathrm{d}x\, \mathrm{d}z. \quad (2)$$

Following [5], the blurred projections are filtered in Fourier space using the regularized inverse of the projected PSF:

$$H_{inv}(\omega_x, \omega_y) = \frac{\mathcal{F}^{2*}\left\{h_{\perp}(x, y)\right\}}{\left|\mathcal{F}^2\left\{h_{\perp}(x, y)\right\}\right|^2 + \lambda\left|\mathcal{F}^2\left\{r(x, y)\right\}\right|^2}, \quad (3)$$

where $\mathcal{F}^2$ is the 2D Fourier transform, $\lambda$ is a regularization weight and $r(x, y)$ is a 2D Laplacian high-pass regularization filter. The FBP [3] is then applied to reconstruct the volumetric information.

The filtering step requires to know the PSF of the imaging system. However, experimentally measuring it is a tedious process sensitive to noise, and theoretical models can only give an ideal approximation of the actual optics [6]. Therefore, the PSF used for deconvolution in practice can contain discrepancies that could degrade the quality of the final reconstruction.

### 2.2. FSS-OPT

To overcome the need for using a deconvolution, we propose to use LSFM illumination to truncate the PSF of the system when acquiring the pseudoprojections. The sample is illuminated from the side using a thin light sheet, as illustrated in Figure 1. This eliminates most of the out-of-focus contribution to the images [7], at the expense of more costly and complex optics required to generate the light sheet, as compared to the wide-field illumination for FPS-OPT.

Integrated platforms built for both OPT and LSFM imaging already exist, and most LSFM devices can be extended to integrate OPT modality without modifying the light sheet system [8]. Such platforms could be operated such as to acquire FSS-OPT images without optical hardware modifications.

In the case of FSS-OPT, the pseudoprojection $q(s, y, \theta)$ obtained at an angle $\theta$ is given by:

$$q(s, y, \theta) = \int_{\mathbb{R}} \left[\left(R_{\theta}\left\{f\right\} \cdot T_z\{g\}\right) * h\right](s, y, z)\, \mathrm{d}z, \quad (4)$$

where $g(x, y, z)$ is the LSFM illumination function, $T_z\{\cdot\}$ is a transformation operator translating a function by a distance $z$ along the focal axis, and $*$ is a 3D convolution operator.

The effective imaging PSF is locally equal to the multiplication of the original PSF $h$ with the illumination function $g$, and brings much less out-of-focus information as the light sheet thickness is smaller than the PSF [9]. The pseudoprojections are therefore less blurred, and the FBP (or other X-ray tomography methods) can be directly applied to the acquired images without any deconvolution. As compared to FPS-OPT, this method does not require any prior knowledge on the system's PSF. FSS-OPT shares similarities with multi-view LSFM techniques [10], but requires less heavy computations for reconstruction as no registration or deconvolution are required. Also, the data storage requirements are the same as for OPT.

## 3. PROPOSED SIMULATION METHOD

To evaluate both methods, we simulate the imaging processes with multiple NAs. In order to get a meaningful sample size of at least 0.1 mm with a realistic sampling resolution, the 3D array representing the object must be at least $256 \times 256 \times 256$. A naive implementation of the imaging equations is very slow for 3D arrays of this size, and does not allow to run the simulations in a reasonable time. In the following section, we describe how we optimized the implementation for a major speed up, before presenting the simulation results.

### 3.1. Efficient framework implementation

We use spline-based algorithms from [11] to implement the X-ray transform and FBP. Only a 2D implementation is provided, and looping over the slices of a 3D array is very inefficient. Radon transform and FBP are highly parallel algorithms that greatly benefit from multithreaded implementations and Graphics Processing Unit (GPU) acceleration [12]. Our implementation uses a GPU-accelerated version of the X-ray transform and FBP whose efficiency stems from sharing computations between layers along the rotation axis. This saves both memory and computation time, and gives a 200-fold speed improvement over the initial implementation.

The FPS-OPT simulation is based on Equation 4 which, although compact in appearance, would be very inefficient if implemented as such because the convolution with $h$ would be computed individually for every $z$ and every $\theta$. By explicitly expanding $T_z\{g\}$ and the convolution with $h$ we can reorder the integrals:

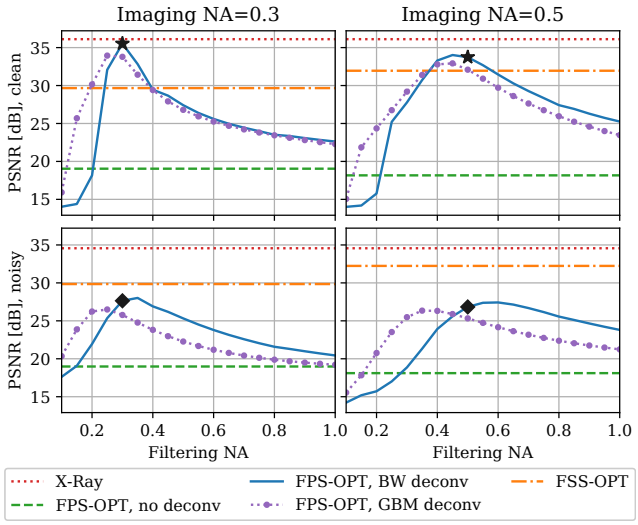


**Fig. 2**. Comparison of the reconstruction PSNR with both methods. Without noise, FPS-OPT beats FSS-OPT if the error on the PSF model is small (★). With Poisson noise, FSS-OPT is better even with perfect PSF knowledge (◆). Ideal X-ray and non-filtered FPS-OPT are shown as anchors.

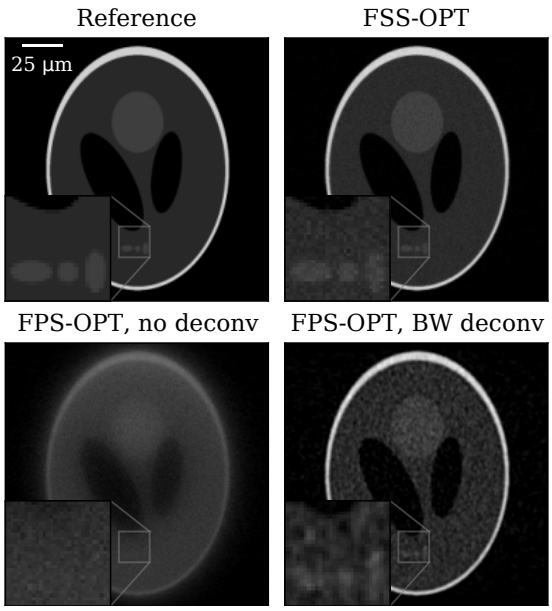


**Fig. 3**. In the presence of Poisson noise, FSS-OPT improves the resolution over FPS-OPT even if the deconvolution PSF is exact. The central $xy$ section of a 3D simulation is shown, imaging NA=0.5.

$$q(s,y,\theta) = \int_{\mathbb{R}} \iiint_{\mathbb{R}^3} R_\theta f(u,v,w)\cdot g(u,v,w-z) \cdot h(s-u,y-v,z-w)\,\mathrm{d}u\,\mathrm{d}v\,\mathrm{d}w\;\mathrm{d}z \tag{5}$$

$$= \iiint_{\mathbb{R}^3} R_\theta f(u,v,w) \int_{\mathbb{R}} g(u,v,w-z) \cdot h(s-u,y-v,z-w)\,\mathrm{d}z\;\mathrm{d}u\,\mathrm{d}v\,\mathrm{d}w \tag{6}$$

$$= \iint_{\mathbb{R}^2} \int_{\mathbb{R}} R_\theta f(u,v,w)\,\mathrm{d}w \int_{\mathbb{R}} g(u,v,\alpha) \cdot h(s-u,y-v,-\alpha)\,\mathrm{d}\alpha\;\mathrm{d}u\,\mathrm{d}v \tag{7}$$

The variable substitution $\alpha = w - z$ between (6) and (7) is valid under the hypothesis that the object has a finite extent in space. The integral over $w$ can then be computed on a finite ensemble $D \subset \mathbb{R}$. We obtain a new formulation for the FSS-OPT pseudoprojection:

$$q(s,y,\theta) = \iint_{\mathbb{R}^2} \mathcal{X}f(u,v,\theta)\cdot h_\perp^{uv}(s,y)\,\mathrm{d}u\,\mathrm{d}v, \tag{8}$$

were we use a local projected PSF $h_\perp^{uv}(x,y)$ defined as:

$$h_\perp^{uv}(x,y) = \int_{\mathbb{R}} g(x,y,z)\cdot h(u-x,v-y,-z)\,\mathrm{d}z. \tag{9}$$

The expression derived above for $q(s,y,\theta)$ yields a very efficient implementation, as the optimized X-ray transform can be used to compute $\mathcal{X}f$. Moreover, the number of total operations is divided by $N_z$, the depth of the object array. As $h_\perp^{uv}$ does not depend on $\theta$, the computation of the local projected PSF can be shared between all angles. This formulation is also suitable for multithreading and GPU acceleration, making its implementation very efficient.

### 3.2. Simulation results

To compare the performance of FPS-OPT and FSS-OPT, we simulated the imaging processes on a 3D Shepp-Logan phantom. We used the Born & Wolf (BW) model [13, 14] to generate the PSFs. The LSFM illumination was simulated to match the OpenSPIM platform [15] using Fresnel propagation in POPPY [16], and the beam thickness and shape were validated by comparison with [17]. The projections were simulated for 360 angles evenly spaced between 0° and 180°. We first considered a noise-free scenario, and then added shot noise modelled by a Poisson distribution on the noise-free data rescaled to the range $[3, 10^4]$.

To quantify the impact of incorrect PSF on FPS-OPT reconstruction, we used multiple PSFs with varying NAs between 0.1 and 1 for deconvolution. We also used an approximated Gaussian Beam Model (GBM) as defined in [18] to account for errors in the model itself. We used the Peak Signal-to-Noise Ratio (PSNR) as criterion for the quality $\mathrm{PSNR} = 10\log_{10}\left(\max(f)^2/\mathrm{MSE}\right)$, where MSE is the Mean Squared Error between the reconstruction and the original object $f$. We used multiple values of $\lambda$ in the inverse filter, and selected the reconstructions with the best PSNR.

Figure 2 compares the reconstruction PSNR for imaging NAs of 0.3 and 0.5, in the ideal noise-free situation (row 1) and in the presence of Poisson noise (row 2). Ideal X-ray (imaging without PSF blurring) represents the best possible reconstruction, while FPS-OPT without deconvolution is the basic scanning OPT. On noise-free images, FPS-OPT outperforms FSS-OPT if the NA of the deconvolution PSF is within 0.1 of the imaging NA, the performance being only slightly reduced when using the GBM approximation. When Poisson noise is added, FSS-OPT outperforms FPS-OPT even if the deconvolution PSF exactly matches the imaging one, yielding a much better resolution in the reconstruction as shown in Figure 3.

## 4. EXPERIMENTS

To validate the simulation results, we imaged two fluorescent textile fibres with a diameter of 25 µm using an OpenSPIM system, with a

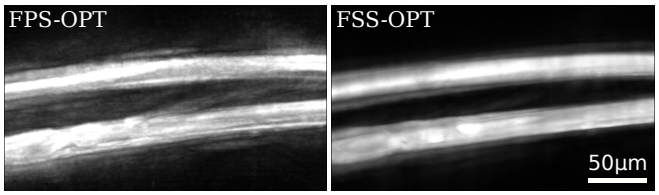


**Fig. 4**. Comparison of FPS-OPT and FSS-OPT on fluorescent textile fibres. Mean intensity projection of the 3D image is shown.

10×/0.5 water dipping objective. The fibres were mounted in a 1.5% low melting agarose solution, inside a fluorinated ethylene propylene tube. We acquired 180 pseudoprojections over 180° by scanning the focal plane over a depth of 300 µm. FPS-OPT was deconvolved with the BW PSF model with a 0.5 NA matching the objective. As visible in Figure 4, FSS-OPT contains less out-of-focus blur than FPS-OPT, which validates the simulation results.

## 5. CONCLUSIONS

We have introduced a simulation framework for FPS-OPT that is flexible and efficient enough to accomodate various 3D illumination geometries. In particular, we proposed FSS-OPT, a scanning OPT imaging technique that reduces the out-of-focus blur using an LSFM illumination, which our simulation framework allowed us to characterize on real-scale 3D data. Our simulations have shown that FSS-OPT outperforms FPS-OPT when Poisson noise is present, improving the resolution without requiring any prior knowledge on the imaging PSF. Furthermore, we have validated the simulated results using experimentally-acquired data. Our simulation framework allowed to identify and characterize the benefits of an alternative all-optical illumination geometry (FSS-OPT).

The source code of the simulation framework is available at `https://github.com/idiap/cbi_toolbox`.

## 6. COMPLIANCE WITH ETHICAL STANDARDS

Experiments use non biological samples for which no ethical approval was required.

## 7. ACKNOWLEDGMENTS

This work has been conducted with the support of the Swiss NSF under grant number 200020_179217: Computational biomicroscopy: advanced image processing methods to quantify live biological systems. The authors declare no competing financial interests.

## References

[1] J. Sharpe, U. Ahlgren, P. Perry, B. Hill, A. Ross, J. Hecksher-Sørensen, R. Baldock, and D. Davidson, "Optical projection tomography as a tool for 3D microscopy and gene expression studies," *Science*, vol. 296, no. 5567, pp. 541–545, 2002.

[2] Q. Miao, J. Hayenga, M. G. Meyer, T. Neumann, A. C. Nelson, and E. J. Seibel, "Resolution improvement in optical projection tomography by the focal scanning method," *Optics letters*, vol. 35, no. 20, pp. 3363–3365, 2010.

[3] A. C. Kak, M. Slaney, and G. Wang, "Principles of computerized tomographic imaging," *Medical Physics*, vol. 29, no. 1, pp. 107–107, 2002.

[4] S. Kikuchi, K. Sonobe, L. S. Sidharta, and N. Ohyama, "Three-dimensional computed tomography for optical microscopes," *Optics communications*, vol. 107, no. 5-6, pp. 432–444, 1994.

[5] K. G. Chan and M. Liebling, "Direct inversion algorithm for focal plane scanning optical projection tomography," *Biomedical optics express*, vol. 8, no. 11, pp. 5349–5358, 2017.

[6] J. G. McNally, T. Karpova, J. Cooper, and J. A. Conchello, "Three-dimensional imaging by deconvolution microscopy," *Methods*, vol. 19, no. 3, pp. 373–385, 1999.

[7] J. Huisken, J. Swoger, F. Del Bene, J. Wittbrodt, and E. H. Stelzer, "Optical sectioning deep inside live embryos by selective plane illumination microscopy," *Science*, vol. 305, no. 5686, pp. 1007–1009, 2004.

[8] A. Bassi, B. Schmid, and J. Huisken, "Optical tomography complements light sheet microscopy for in toto imaging of zebrafish development," *Development*, vol. 142, no. 5, pp. 1016–1020, 2015.

[9] C. J. Engelbrecht and E. H. Stelzer, "Resolution enhancement in a light-sheet-based microscope (SPIM)," *Optics letters*, vol. 31, no. 10, pp. 1477–1479, 2006.

[10] J. Swoger, P. Verveer, K. Greger, J. Huisken, and E. H. Stelzer, "Multi-view image fusion improves resolution in three-dimensional microscopy," *Optics express*, vol. 15, no. 13, pp. 8029–8042, 2007.

[11] S. Horbelt, M. Liebling, and M. Unser, "Discretization of the Radon transform and of its inverse by spline convolutions," *IEEE Transactions on medical imaging*, vol. 21, no. 4, pp. 363–376, 2002.

[12] A. Fasih and T. Hartley, "GPU-accelerated synthetic aperture radar backprojection in CUDA," in *2010 IEEE Radar Conference*, IEEE, 2010, pp. 1408–1413.

[13] M. Born and E. Wolf, *Principles of optics: electromagnetic theory of propagation, interference and diffraction of light*. Elsevier, 2013, ch. 8.

[14] H. Kirshner, F. Aguet, D. Sage, and M. Unser, "3-D PSF fitting for fluorescence microscopy: Implementation and localization application," *Journal of microscopy*, vol. 249, no. 1, pp. 13–25, 2013.

[15] P. G. Pitrone, J. Schindelin, L. Stuyvenberg, S. Preibisch, M. Weber, K. W. Eliceiri, J. Huisken, and P. Tomancak, "OpenSPIM: An open-access light-sheet microscopy platform," *nature methods*, vol. 10, no. 7, p. 598, 2013.

[16] M. Perrin, J. Long, E. Douglas, A. Sivaramakrishnan, and C. Slocum, "POPPY: Physical Optics Propagation in PYthon," *ascl*, ascl–1602, 2016.

[17] E. Remacha, L. Friedrich, J. Vermot, and F. O. Fahrbach, "How to define and optimize axial resolution in light-sheet microscopy: A simulation-based approach," *Biomedical Optics Express*, vol. 11, no. 1, pp. 8–26, 2020.

[18] A. K. Trull, J. van der Horst, W. J. Palenstijn, L. J. van Vliet, T. van Leeuwen, and J. Kalkman, "Point spread function based image reconstruction in optical projection tomography," *Physics in Medicine & Biology*, vol. 62, no. 19, p. 7784, 2017.